The Macroscopic Elasticity of 3D Woven Composites

B. N. COX* AND M. S. DADKHAH
Rockwell Science Center
1049 Camino Dos Rios
Thousand Oaks, CA 91360

(Received March 21, 1994)
(Revised September 4, 1994)

ABSTRACT: The elastic properties of graphite/epoxy composites with three-dimensional interlock weave reinforcement have been measured over length scales somewhat greater than the characteristic length of the weave pattern. Orientation averaging models similar to those developed elsewhere over the last twenty years provide estimates of elastic constants that are in fair agreement with the experimental data. However, in-plane Young's moduli are consistently too high and properties related to the through-thickness reinforcement show considerable scatter. Most of the discrepancies can be attributed to waviness and other geometrical irregularities in nominally straight tow segments. Much improved agreement with in-plane properties is obtained by measuring and accounting for the out-of-plane waviness of in-plane tows. Other observed distortions of in-plane tows and irregularity in through-thickness tows are very difficult to quantify experimentally. There results a significant and apparently unavoidable uncertainty in predictions of properties that depend strongly on the through-thickness reinforcement. Nevertheless, the utility of orientation averaging models in applications where the in-plane properties are paramount is clearly verified.

1. INTRODUCTION

TEXTILE COMPOSITES WITH three-dimensional (3D) reinforcement possess some remarkable mechanical properties. In skin applications, 3D woven or braided composites and stitched laminates are invulnerable to failure by delamination and buckling, provided the through-thickness reinforcement is not distorted during fabrication [1–13]. The through-thickness reinforcement limits delamination and damage extension after impact, allowing compressive strength often to remain comparable to that of pristine material. Like 3D carbon-carbon composites of earlier years [3], 3D woven polymer composites possess exceptionally high strain to failure in either compression or tension [12–14]. In work

*Author to whom correspondence should be addressed.

0021-9983/95/06 785-35 $10.00/0

of fracture and notch insensitivity in tension, they far surpass metal alloys and conventional polymer laminates [13,14].

Detailed experimental observations on 3D woven composites have revealed that the reinforcement geometry has a dominant role in determining mechanisms of failure [12–15]. Both the ideal composite geometry, in which in-plane tows are straight, and deviations from the ideal are important. In fact, high stress to failure, notch insensitivity, and damage tolerance can all be attributed to the presence of geometrical flaws in the reinforcement [12–14]. Some geometrical flaws consist of certain local configuration of tows, such as sites where through-thickness yarns wrap around nominally straight in-plane yarns. Other geometrical flaws are segments of in-plane tows that are misaligned to an unusually high degree.

Properties related to failure, including strength and the degree of localization of damage, are sensitive to flaw statistics, especially the number and spatial distribution of extreme flaws. In the elastic regime, on the other hand, the effects of geometrical irregularity ought to be more moderate. Elastic constants measure a spatially averaged response, in which extremes carry only a small weight. Thus in Reference [13] it was shown that Young's modulus in the primary load-bearing direction of 3D woven composites can be predicted well by combining rules of mixtures with crude estimates of the effects of random tow misalignment or waviness. In fact, the 3D woven composites studied in References [12–15] behave in the elastic regime much like laminates. The idea of simple models for elastic constants is pursued here in a complete description of the elastic properties of the same class of 3D woven composites.

The emphasis in this paper is on predicting macroscopic composite elastic properties, i.e., properties applicable over gauge lengths larger than the characteristic scale of the pattern of tows in the reinforcement. Experimental methods are developed for characterizing the waviness of nominally straight tows, which are in practice far from straight. Tow waviness leads to reduction of the effective axial modulus of a single tow. A simple estimate of this softening is then incorporated in a model of the composite, in which spatially averaged composite properties are estimated by averaging the properties of constituent tows of different orientations.

The simple approach espoused in this paper follows orientation averaging models presented for 3D composites many years ago [16–18]. More recent variants appear in References [19] and [20]. The primary goal of this paper is to test how well macroscopic elastic constants can be predicted by such approximations for the current generation of 3D woven composite panels, provided tow irregularity is accounted for in an appropriate, spatially averaged way. Computationally, the models require nothing more than the inversion of a 9×9 matrix. Conceptually, they have the immense advantage of simplicity, which should be contrasted with the large computations that follow from finite element formulations of the same task.

While the simple approach works very well for predicting the in-plane macroscopic properties of flat panel specimens, in other problems a more complete description of the stress distribution throughout the composite is required. Im-

portant problems of this class include modeling the elastic properties of three-dimensionally reinforced parts of complex shape; and analyzing the random distribution of loads in individual reinforcing tows when the tows are irregular. For these problems, finite element or similarly laborious computations are inevitable. The formulation of a new finite element model called the "Binary Model," which is designed to deal most efficiently with these and other problems, was presented in Reference [21]. In Reference [22], the calibration of the Binary Model for elastic problems is described in full and it is used to model statistical aspects of the composites studied here.

2. MATERIALS

Analyses will be presented for the eleven woven interlock composites studied in References [12–15]. Figure 1 shows the three types of weave in this group,

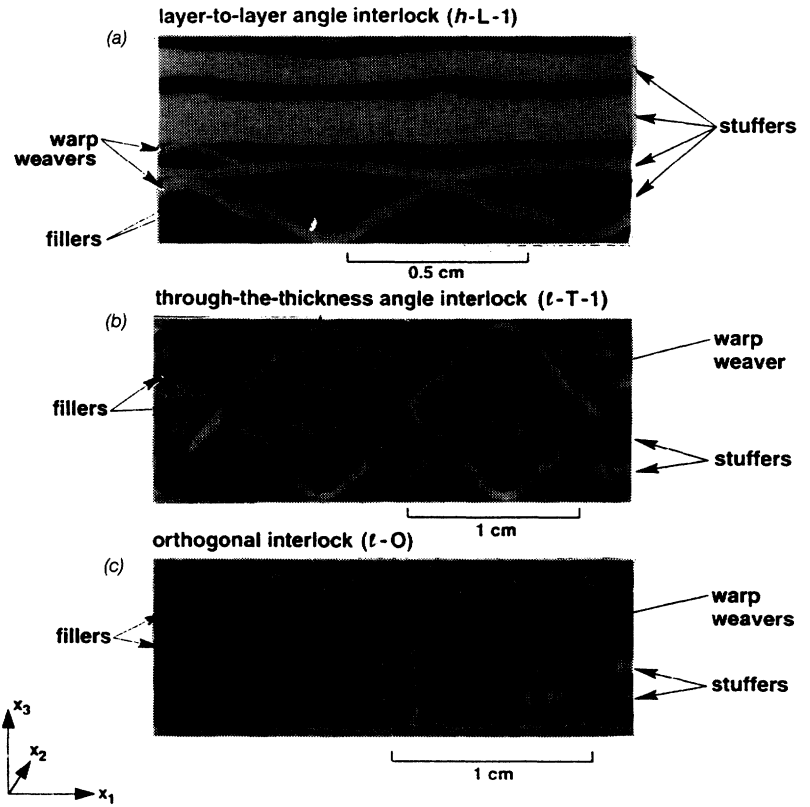

Figure 1. *Sections normal to the filler direction of specimens with three different weave types. Stuffers and warp weavers appear as light ribbons. Sections of fillers appear as dark patches.*

namely layer-to-layer and through-the-thickness angle interlock and orthogonal interlock weaves. "Stuffer" and "filler" tows form an orthogonal array suggestive of a course 0°/90° laminate, while "warp weaver" tows provide through-thickness reinforcement. Further notes on weave patterns are given in Appendix A and complete specifications in Reference [22]. In the jargon of crystallographers, all the weaves are orthorhombic in the absence of any tow distortions. The orthogonal interlock weaves are also invariant under certain inversions; but not the angle interlock weaves, as contemplation of the detailed drawings in Reference [22] will reveal.

The subject composites can also be classified by the total fiber volume fraction, V_f achieved in processing: "lightly compacted" composites, with relatively low V_f and "heavily compacted" composites, with relatively high V_f. Table 1 reintroduces labels from Reference [13] for the 11 composites studied, with the italic letter designating the degree of compaction (l for light and h for heavy).

The layers in Figure 1 are much thicker than plies in a conventional 2D laminate, because the individual tows are ~ 1 mm^2 in cross section. Such coarseness lowers manufacturing cost, which rises with the number of yarns to be set up on the loom. Fortunately, it also favors damage tolerance and notch insensitivity [13,14].

Nearly all the composites of Table 1 consist of AS4 carbon fibers[1] in epoxy resin. The exceptions are composites l-L-2 and l-T-2, in which the warp weavers were S-glass fibers. All lightly consolidated composites were made with Tactix 138 resin cured with H41 hardener;[2] all heavily compacted composites were made with Shell RSL-1895 resin with EPON CURING AGENT® W.[3] Further processing details appear in References [12] and [13].

Table 1 also lists for each composite the weaver's specifications of the linear density of yarns in the loom (ends per unit length, e, and picks per unit length, p) and the yields (length per unit mass) y_α, $\alpha = s, f,$ or w for stuffers, fillers, or warp weavers. (The symbol α will be used throughout this paper to identify tow type in the weave.)

2.1 Fiber Distributions

Reliable predictions of engineering properties require accurate knowledge of the volume fractions of stuffer, filler, and warp weaver fibers. In principle, these volume fractions could be deduced from the weaver's specifications just listed, together with the measured thickness of the composite. However, this would assume that the mean separation of yarns did not change during manufacture of the composite, which may be optimistic.[4] In this work, the weaver's specifications were used only to deduce the fractions by volume f_α ($\alpha = s, f,$ or w) of all fibers that lie in stuffers, fillers, and warp weavers.[5] All macroscopic elastic properties

[1]Hercules Inc., Salt Lake City, Utah.
[2]Dow Chemical Co., Freeport, Texas.
[3]Shell Oil Co., Anaheim, California.

Table 1. Composite and fiber data.

Composite Label	Architecture	Tow Yield			Linear Tow Density		Crimp Factor
		Stuffers y_s (mm/g)	Fillers y_f (mm/g)	Weavers y_w (mm/g)	Stuffers e (mm^{-1})[a]	Fillers p (mm^{-1})[b]	c_w
(a) Lightly Compacted							
l-L-1	Layer-to-Layer	652	652	1525	0.51	0.44	1.2[c]
l-L-2	Angle Interlock	652	652	1510	0.51	0.59	1.2[c]
l-T-1	Through-the-Thickness	652	652	1525	0.47	0.50	1.4[c]
l-T-2	Angle Interlock	652	652	1510	0.51	0.50	1.4[c]
l-O	Orthogonal Interlock	652	652	1525	0.47	0.51	3.25[c]
(b) Heavily Compacted							
h-L-1	Layer-to-Layer	570	1140	(2280, 13600)[d]	0.55	0.51	1.2
h-L-2	Angle Interlock	1140	2280	(4570, 13600)[d]	0.71	0.79	1.03
h-T-1	Through-the-Thickness	570	1140	2280	0.55	0.51	1.375
h-T-2	Angle Interlock	1140	2280	4570	0.71	0.79	1.25
h-O-1	Orthogonal Interlock	570	1140	2280	0.55	0.51	4
h-O-2	Orthogonal Interlock	1140	2280	4570	0.71	0.79	4.5

[a]"Ends per cm" ≡ number of columns of stuffers per cm in the weft direction.
[b]"Picks per cm" ≡ number of columns of fillers per cm in the warp direction.
[c]Estimated, not measured.
[d]The first figure refers to warp weavers, the second to surface warp weavers (see Appendix A).

are deduced from these fractions, the measured total fiber volume fraction, V, and the measured composite thickness, t.

In a composite with n_s layers of stuffers alternating with $n_s + 1$ layers of fillers through the thickness, n_w warp weavers between successive columns of stuffers (see Appendix A and Reference [22]), and in which all yarns are made of the same fibers

$$f_s = \frac{n_s e c_s}{L y_s} \; ; \quad f_f = \frac{(n_s + 1) p c_f}{L y_f} \; ; \quad f_w = \frac{n_w e c_w}{L y_w} \tag{1}$$

where c_s, c_f, and c_w are crimp factors; L is chosen to satisfy $f_s + f_f + f_w = 1$; and y_w is an appropriately weighted average for composites with warp weavers and surface warp weavers of unequal yields (composites h-L-1 and h-L-2). The crimp factors are customarily determined by measuring the lengths of yarns extracted from a representative length of woven preform. Both c_s and c_f are very close to unity. Values of c_w supplied by the weaver are given in Table 1. (For the lightly compacted composites, which were the first manufactured [12], crimp factors could not be found in old records. Estimates have been substituted. Since the warp weavers constitute a relatively small fraction of all reinforcement, the effect on f_s and f_f and therefore on predicted in-plane properties of any error in c_w is negligible compared to other factors, especially softening due to waviness. However, see below for the effects on out-of-plane properties. The only additional measurement required to fix the density of reinforcement in a composite containing a single type of fiber is the total fiber volume fraction, V.

In a composite in which the warp weavers contain different fibers from those in the stuffers and fillers (composites l-L-2 and l-T-2), f_w is determined by a separate experimental measurement of the volume fraction, V', of weaver fibers (S2 glass here): $f_w = V'/(V + V')$. In this case only f_s and f_f are defined by Equation (1), with L chosen to satisfy $f_s + f_f = V/(V + V')$.

Table 2 shows values of f_s, f_f, and f_w computed by these rules, along with measured values of V and, where appropriate, V'.

In estimating flexural rigidity, information is also required of the distribution of stuffers and fillers through the thickness of the composites. Let t_f and t_s denote the thicknesses of filler and stuffer layers, with all filler layers assumed equal and all stuffer layers assumed equal (Figure 2). (Generalization to unequal layers of stuffers or fillers, which might be preferred to maximize flexural rigidity in one direction, follows obviously.) Assuming equal degrees of compaction of stuffers and fillers,

$$\frac{t_s}{t_f} = \frac{y_f e}{y_s p} \tag{2a}$$

[4]Total fiber volume fractions estimated for the heavily compacted composites from the weaver's specifications and the measured composite thickness were found to be consistently higher than measured values by up to 5%.

[5]It will be assumed here that stuffers and fillers spread equally during consolidation. This assumption is reasonable in manufacturing flat panels. When preforms are deformed to make curved parts, especially those involving nondevelopable transformations, tows are likely to thin or consolidate anisotropically. The analysis of such cases is a current research topic.

Table 2. Composite volume fractions and dimensions.

Composite Label	Fraction by Volume of All Fibers That Lie in: Stuffers f_s	Fillers f_f	Weavers f_w	Measured Fiber Volume Fraction[a] V (V')	Composite Thickness t (mm)
(a) Lightly Compacted					
l-L-1	0.385	0.418	0.197	0.35 ± 0.03	12.6
l-L-2	0.347	0.502	0.151	0.370 ± 0.005[b] (0.066 ± 0.004[c])	12.4
l-T-1	0.381	0.504	0.115	0.466 ± 0.003	10.2
l-T-2	0.406	0.497	0.097	0.408 ± 0.020[b] (0.044 ± 0.004[c])	9.7
l-O	0.387	0.524	0.090	0.483 ± 0.010	8.8
(b) Heavily Compacted					
h-L-1	0.587	0.340	0.073	0.620 ± 0.008	5.61
h-L-2	0.580	0.375	0.045	0.557 ± 0.015	6.25
h-T-1	0.571	0.331	0.098	0.613 ± 0.003	5.73
h-T-2	0.571	0.369	0.059	0.592 ± 0.014	5.77
h-O-1	0.586	0.340	0.073	0.619 ± 0.008	5.79
h-O-2	0.545	0.353	0.102	0.593 ± 0.014	5.87

[a]Measured by acid digestion following ASTM Standard D3171.
[b]Graphite fibers.
[c]Glass fibers.

$$(n_s + 1)t_f + n_s t_s = t \tag{2b}$$

where t denotes the measured composite thickness (Table 2). Hence

$$t_f = \frac{y_s p t}{(n_s + 1)y_s p + n_s y_f e} \tag{3a}$$

$$t_s = \frac{y_f e t}{(n_s + 1)y_s p + n_s y_f e} \tag{3b}$$

In the coordinate system of Figure 2, the layers of the upper half of the stack have the boundaries $u_o = 0$ and

$$u_i = \begin{cases} \frac{i}{2}t_f + \frac{i-1}{2}t_s & (n_s i \text{ odd}) \\ \frac{i-1}{2}t_f + \frac{i}{2}t_s & (n_s i \text{ even}) \end{cases} \qquad (i = 1,\ldots,n_s + 1) \tag{4}$$

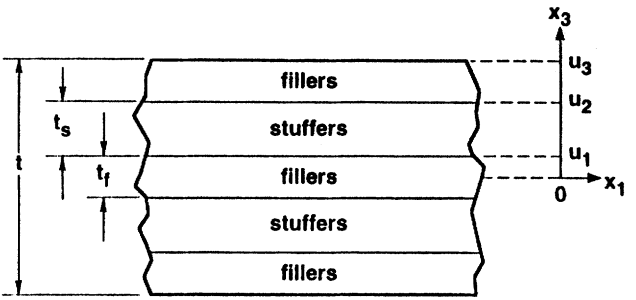

Figure 2. *Representative layer sequence of fillers and stuffers through the thickness, with the layer thicknesses* t_f *and* t_s *defined. For the case shown,* $n_s = 2$.

2.2 Tow Waviness

In contradiction of the ideal geometry prescribed by the weaver and widely assumed in prior modeling of textile composites, stuffers and fillers are in reality not straight. Indication of this for stuffers is visible in Figure 1: the stuffers exhibit appreciable deflections in the out-of-plane or through-thickness direction (i.e., in x_1-x_3 planes in Figure 1). Figure 3 shows that such irregularity or

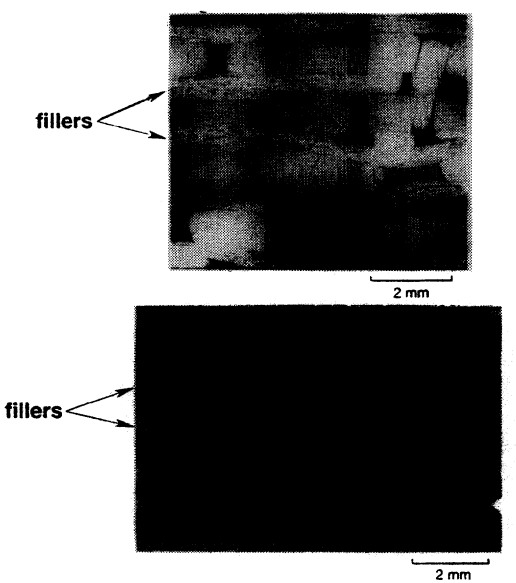

Figure 3. *Sections of two specimens normal to the stuffer direction showing typical irregularity or waviness of fillers, (above: h-L-1; below: h-L-2, showing tow loci calculated by image analysis).*

waviness can be quite dramatic for fillers. It is generally larger for fillers than stuffers because the stuffers, being warp yarns, are held in tension during weaving, whereas the fillers are non-tensioned weft. In the heavily compacted composites, filler distortion is probably further exacerbated by the fact that fillers are only half as thick as stuffers. Waviness in stuffers and fillers tends to be greater in the lightly compacted composites than in the heavily compacted composites; and greater for angle interlock than for orthogonal interlock weaves.

Warp weavers also exhibit waviness; in some cases, they are the most severely distorted of all the tows. Warp weaver irregularity is generally more pronounced in angle interlock than in orthogonal interlock composites. It is also closely correlated with the reduction in thickness of the woven preform during consolidation of the composite [13], as should be expected. Some examples of warp weaver crimp appear in Figure 4 (see also Figure 4 of Reference [13]).

There is also some in-plane misalignment of stuffers and fillers, i.e., in the x_1-x_2 plane. However, these fluctuations are considerably smaller than out-of-plane misalignments and are neglected in all the following analyses.

OUT-OF-PLANE WAVINESS OF STUFFERS AND FILLERS

Out-of-plane waviness was quantified by statistical analysis of digitized images of cross sections.[6] Digital image analysis was used to reduce images of stuffers and fillers such as those in Figures 1 and 3 to one-dimensional curves or "tow loci" representative of their centers. Typical tow loci are shown superimposed on the fillers of Figure 3. The analysis of elastic properties requires data on the distribution of out-of-plane misalignment angles along the entire length of tows. The analysis of strength and fatigue life requires distributions of extreme values [13,15].

Considerable effort was expended in finding the best method of generating and smoothing tow loci. Details of the procedure finally selected are as follows. Cross sectional images were first digitized on 256 × 256 arrays. The size of the area on the specimen represented by a single pixel depended on the image magnification. A gray level threshold was then used to delineate individual tows. The representation of each tow identified in this manner was skeletonized by alternately eliminating pixels from the upper and lower boundaries. The coordinates of the centers of mass of the surviving pixels in the skeletons were stored for subsequent analysis as the raw tow loci data. Subjectivity entered in the procedure to this point only in a small amount of touching up to aid in contrast thresholding and the elimination of some spurious features associated with fragments of tows caught on the specimen section.

The first step in deducing misalignments from the raw tow loci data was to eliminate noise arising from the digital image processing. The noise consisted of steps corresponding to the pixel size (Figure 5). In such stepped data, the most accurately known values are the midpoints of the vertical segments. Smoothing was therefore effected by fitting cubic splines to the set of all step midpoints on

[6]Similar analysis of waviness in triaxial braids can be found in References [23] and [24].

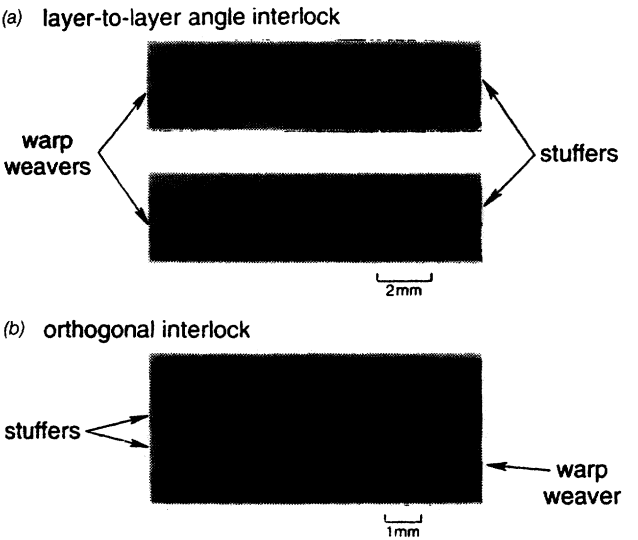

Figure 4. *Sections normal to the filler direction showing warp weaver crimp in two heavily compacted composites.*

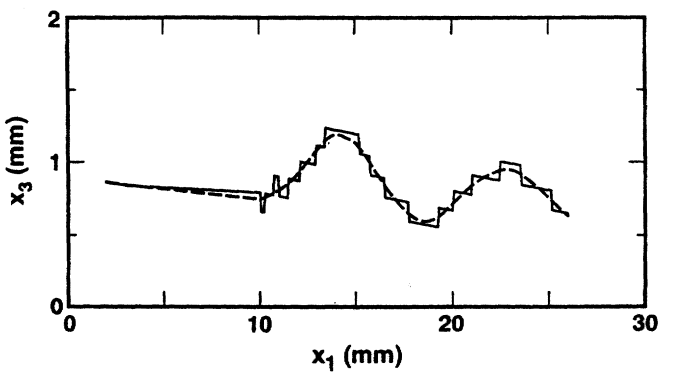

Figure 5. *Steps on a digitized tow locus reflecting the size of pixels in the digitized image (solid curve); and a smoothing spline function (dashed curve).*

each locus. The fitting routine used[7] finds splines of minimum curvature such that the root mean square difference between the fitted splines and the data points does not exceed some specified amount δ. Forcing the splines to pass exactly through the data ($\delta = 0$) results in large oscillations or ringing as the splines accommodate noise. Specifying a very large value of δ results in lost information, with the fitted spline tending to a straight line. The optimal choice of δ should correspond to the expected error in each datum. The error should be a small fraction of the step height, but it is difficult to specify a priori. Therefore, the optimal value of δ was determined by comparing fitted splines with the original micrographs by eye. Acceptable fits were found when $\delta = 0.02 \pm 0.01$ mm, or about one fifth of the step height (Figures 3 and 5). The fitted curves were considerably superior to smoothed curves obtained by filtering Fourier transforms.

To check the adequacy of the pixel density, some cross sections were analyzed again starting with images of higher magnification. The step size was accordingly smaller. With δ again set to one fifth the average step size, smoothed curves close to those obtained from the lower magnification images were generated.

At least five sections were analyzed for each material. A cumulative probability distribution (cpd) was then formed for the out-of-plane misalignment angle, ξ, of small, equal intervals on all smoothed tow loci. Typical cpds are shown in Figure 6. Although there are no obvious physical grounds to expect it, experience shows that each such cpd can be fitted quite well by a symmetric normal distribution

$$F_\xi(\xi) = \int_{-\infty}^{\xi} f_\xi(\xi')\,d\xi' \tag{5a}$$

with the density function $f_\xi(\xi)$ given by

$$f_\xi(\xi) = \frac{1}{\sigma_\xi\sqrt{2\pi}} e^{-\xi^2/2\sigma_\xi^2} \tag{5b}$$

Typical fitted functions $F_\xi(\xi)$ are also shown in Figure 6. The width, σ_ξ, of the distributions determines the degree of softening of Young's modulus in the tow direction due to out-of-plane tow waviness (see below). Values of σ_ξ determined by maximum likelihood estimators are listed in Table 3.

The influence of uncertainty in the smoothing parameter δ was assessed by reevaluating σ_ξ using the lowest and highest credible values assigned to δ. The resulting uncertainty in σ_ξ is also indicated in Table 3. For stuffers, it is typically $\sim 30\%$; for fillers, $\sim 10\%$. Higher (lower) values of δ lead to narrower (broader) distributions of ξ. However, as long as δ is varied consistently for all cases, the net effect is broadening or narrowing of all distributions by the same factor. The

[7]IMSL (International Mathematical Software Library) routine ICSCSU.

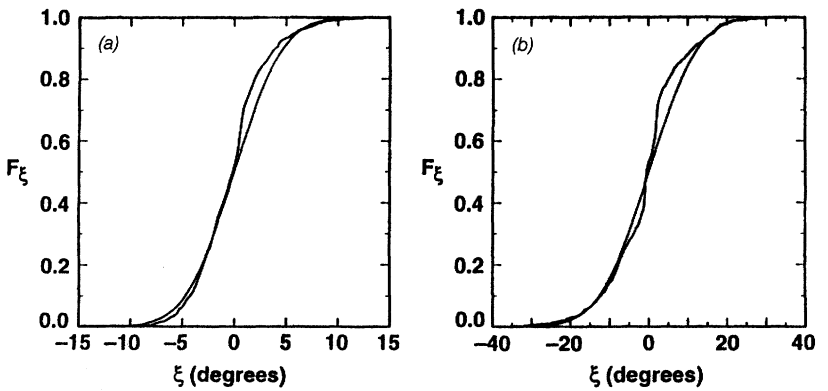

Figure 6. *Distributions of the out-of-plane misalignment angle ξ for (a) stuffers in the composite I-T-2 and (b) fillers in the composite I-L-2. The irregular curves are the data; the overlaid smooth curves show symmetric normal distributions fitted by maximum likelihood estimators.*

relative uncertainty in σ_ξ for different composites may therefore be much less than the uncertainty shown in Table 3. From statistical arguments, it should fall as the square root of the number of data points sampled [25]. When the data available for the stuffers in each composite were analyzed in two halves, the two values of σ_ξ obtained differed typically by 10%. This is a better estimate of the *relative* uncertainty in out-of-plane misalignment angles for stuffers.

CRIMP OF WARP WEAVERS

The distortion of warp weavers is much more difficult to quantify. Warp weavers follow complicated paths and are often much more severely crimped than stuffers or fillers (Figure 4). Warp weavers, being of lighter denier, also exhibit greater departures proportional to their widths from the planes in which they nominally lie. Therefore specimen sections rarely display cleanly defined outlines of warp weavers. Warp weavers fade in and out of exposed sections and are often fragmented by the cutting action.

It was not possible to obtain realistic statistics for warp weaver misalignment angles, however these might be defined. Instead, a qualitative assessment of the degree of crimp was made by inspecting images of cross sections such as Figure 4. The degree of crimp is manifestly correlated with the extent to which the dry fiber preform was squashed in consolidating the composite (Table 3): compare the heavily compacted composite of Figure 4(a) with the lightly compacted composite of Figure 1(b).

3. ELASTIC CONSTANTS

3.1 Experimental Data

Since the warp weavers generally contain a small fraction of the total fibers, the

Table 3. Tow waviness parameters.

Composite Label	σ_ξ (degrees)		Stiffness Knockdown Factor $\eta^{(\alpha)}$		Degree of Warp Weaver Crimp	Composite Thickness/ Preform Thickness
	Stuffers	Fillers	Stuffers	Fillers		
l-L-1	—[a]	—[a]	—	—	severe	—[b]
l-L-2	4.0 ± 1.0	9.9 ± 0.8	0.82 ± 0.07	0.45 ± 0.04	severe	—
l-T-1	3.4 ± 0.8	6.0 ± 0.6	0.86 ± 0.06	0.66 ± 0.04	intermediate	—
l-T-2	3.7 ± 0.7	6.4 ± 0.8	0.84 ± 0.05	0.64 ± 0.05	intermediate	—
l-O	3.4 ± 0.8	1.2 ± 1.0	0.86 ± 0.06	0.98 ± 0.05	severe	—
h-L-1	1.7 ± 0.5	4.8 ± 0.7	0.97 ± 0.02	0.69 ± 0.06	severe	0.79
h-L-2	2.0 ± 0.6	14.8 ± 0.8	0.95 ± 0.02	0.32 ± 0.02	severe	0.75
h-T-1	1.3 ± 0.5	2.9 ± 0.7	0.98 ± 0.02	0.91 ± 0.04	intermediate	0.83
h-T-2	1.7 ± 0.3	4.2 ± 1.0	0.97 ± 0.02	0.83 ± 0.06	slight	0.93
h-O-1	0.3 ± 0.1	3.4 ± 0.7	0.99 ± 0.01	0.89 ± 0.05	intermediate	0.87
h-O-2	1.2 ± 0.6	1.8 ± 1.0	0.98 ± 0.02	0.97 ± 0.06	slight	0.91

[a]This preform was so inhomogeneously distorted that meaningful measurements of F_ξ could not be made.
[b]Not known for lightly compacted composites.

reinforcement is dominated by the orthogonal arrays of stuffers and fillers and is therefore approximately orthotropic. Detailed modeling confirms orthotropic symmetry over gauge lengths exceeding several tow diameters, even in the presence of local irregularities in tow positioning [22]. Therefore, macroscopic elastic properties are given by nine Voigt elastic constants, C_{ij}. With x_1 lying in the stuffer direction, x_2 in the filler direction, and x_3 in the through-thickness direction.

$$\begin{vmatrix} \sigma_1 \\ \sigma_2 \\ \sigma_3 \\ \tau_{23} \\ \tau_{31} \\ \tau_{12} \end{vmatrix} = \begin{vmatrix} C_{11} & C_{12} & C_{13} & 0 & 0 & 0 \\ C_{21} & C_{22} & C_{23} & 0 & 0 & 0 \\ C_{31} & C_{32} & C_{33} & 0 & 0 & 0 \\ 0 & 0 & 0 & C_{44} & 0 & 0 \\ 0 & 0 & 0 & 0 & C_{55} & 0 \\ 0 & 0 & 0 & 0 & 0 & C_{66} \end{vmatrix} \begin{vmatrix} \epsilon_1 \\ \epsilon_2 \\ \epsilon_3 \\ \gamma_{23} \\ \gamma_{31} \\ \gamma_{12} \end{vmatrix} \tag{6}$$

The constants C_{ij} are often determined from measurements of Young's modulus and Poisson's ratio for uniaxial loading in each of the directions x_1, x_2, and x_3 together with measurements of the shear moduli G_{23}, G_{31}, and G_{12} [26]:

$$[S_{ij}] = [C_{ij}]^{-1} \tag{7a}$$

$$[S_{ij}] = \begin{vmatrix} 1/E_1 & -\nu_{12}/E_1 & -\nu_{23}/E_1 & 0 & 0 & 0 \\ -\nu_{12}/E_1 & 1/E_2 & -\nu_{23}/E_2 & 0 & 0 & 0 \\ -\nu_{13}/E_1 & -\nu_{23}/E_2 & 1/E_3 & 0 & 0 & 0 \\ 0 & 0 & 0 & 1/G_{23} & 0 & 0 \\ 0 & 0 & 0 & 0 & 1/G_{31} & 0 \\ 0 & 0 & 0 & 0 & 0 & 1/G_{12} \end{vmatrix} \tag{7b}$$

where E_i is Young's modulus for loading in the direction x_i, ν_{ij} is Poisson's ratio for the concomitant contraction in the direction x_j, and use has been made of the symmetry relation

$$\nu_{ij}/E_i = \nu_{ji}/E_j \tag{8}$$

In this work, the engineering constants E_1, E_2, ν_{23}, ν_{31}, and ν_{12} were determined by conducting uniaxial tension tests in the in-plane directions x_1 and x_2. Dog-bone specimens were used in these tension tests, with gauge sections approximately 10 mm × 20 mm × (specimen thickness). The through-thickness modulus E_3 was deduced from tests in which specimens were loaded in compression in the direction x_3 between flat platens. Since the in-plane dimensions of the compression specimens far exceeded their thicknesses, the in-plane strains in the compression tests remained approximately zero. The load-displacement data therefore yielded the stiffness matrix element C_{33}. Young's modulus E_3 was calculated from this value of C_{33} and the measured values of E_1, E_2, and ν_{ij} using Equation (7). Test calculations showed that the uncertainty in E_3 due to measure-

ment errors in the other engineering elastic contants was typically ~5%. Shear moduli were not measured. Some values taken from other work will be used to assess predictive models below.

In many of the tension tests, full-field strain maps were obtained by moiré interferometry. The moiré fringe maps always revealed significant nonuniformity in surface strain distributions. Fringes formed by in-plane displacements (i.e., displacements on x_1-x_2 planes) parallel to the load correspond to the pattern formed by warp weaver extrema at the surface being observed [Figure 7(a)]. The surface is revealed as an approximately periodic pattern of relatively soft and hard patches (shown by locally high or low fringe densities), with lattice parameters commensurate with the tow spacings. However, the pattern is always imperfect: significant, nonperiodic irregularity exists in the details of the strain distributions. In-plane displacements transverse to the load were almost always very small, leading to very sparse fringe systems and indicating very small Poisson's ratios [Figure 7(b)].

Fringes formed by displacements on through-thickness sections by loads in the direction x_1 are typified by Figure 8. Displacements in the loading direction

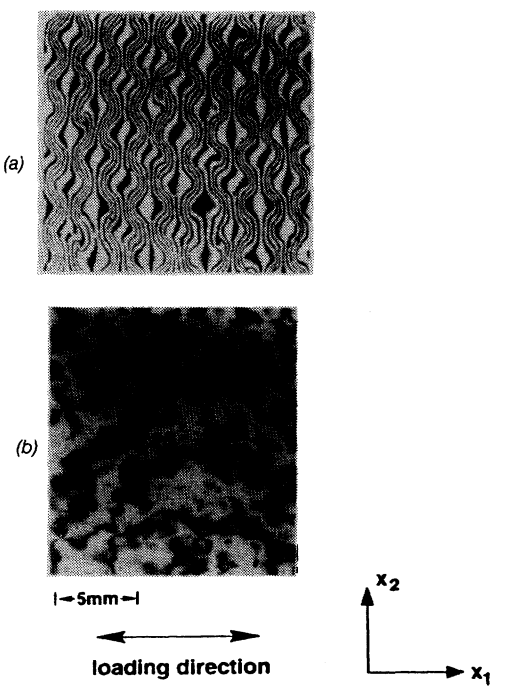

Figure 7. *Moire fringe patterns formed on an in-plane surface (x_1-x_2 plane) of a specimen of composite h-O-2 under uniaxial loading in the direction x_1. (a) Displacement in the direction x_1. (b) Displacement in the direction x_2.*

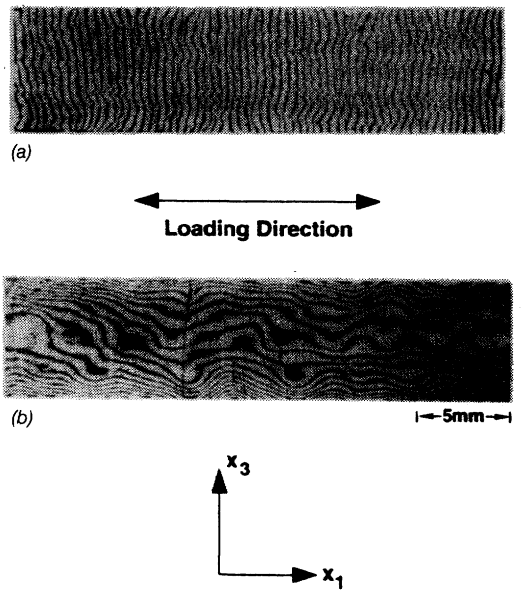

Figure 8. Moire fringe patterns formed on a through-thickness section (x_1-x_3 plane) in a specimen of composite h-L-1 under uniaxial loading in the direction x_1. (a) Displacement in the direction x_1. (b) Displacement in the direction x_3.

reveal fairly uniform strain [Figure 8(a)]; whereas displacements in the through-thickness direction reveal highly nonuniform strain [Figure 8(b)]. Relatively hard areas in Figure 8(b) are directly correlated with warp weavers on the surface being examined.

Taking account of the roughly periodic patterns exemplified by Figure 7(a), in-plane Young's moduli representative of macroscopic strains were obtained by averaging strains over an area of approximately 10 mm × 10 mm. The in-plane Poisson's ratio was deduced from the total displacement across the specimen in the direction of the contraction, averaged over a length of approximately 10 mm along the load axis. The through-thickness modulus E_3 and Poisson's ratio ν_{13} were determined from the total displacement in the through-thickness direction.

The measured elastic constants are reported in Table 4. In a few cases, multiple tests were run to establish representative deviances. For all constants, the deviance was typically 5–10%. Factors contributing to the deviance will be discussed below.

3.2 An Orientation Averaging Model

Macroscopically averaged elastic constants have been estimated in the past for both 2D and 3D composites of stiff, continuous fibers in a soft matrix by simple "orientation averaging" models [16–20]. In these models, small volumes in which

Table 4. Measured and predicted composite elastic constants.

Composite Label	E_1 (GPa)			E_2 (GPa)			E_3 (GPa)		
	Expt.	OA[a]	OAW[b]	Expt.	OA[a]	OAW[b]	Expt.	OA[a]	OAW[b]
l-L-1	30 ± 6	36.8	—		38.7		5.7	9.0	
l-L-2	28.5	34.9	29.4		47.6	22.8	5.9	7.0	6.9
l-T-1	27	47.3	41.3		59.5	40.1	8.0	9.4	9.4
l-T-2	39	43.5	37.1		51.6	34.0	7.9	7.0	7.0
l-O	30 ± 2	51.9	45.4	45.5 ± 1.5	63.9	62.6	7.0 ± 1	13.7	13.7
h-L-1	85 ± 8	91.5	88.6	43.8	56.2	40.8	16 ± 2	12.1	12.1
h-L-2	80	81.2	77.6	42.3	55.0	20.9	14.0	10.2	10.1
h-T-1	79	88.6	87.0	42.5	54.4	50.2	13.8	12.8	12.8
h-T-2	72	85.1	82.4	45.8	57.6	48.8	13.9	11.2	11.2
h-O-1	88	93.1	93.0	39.9	56.4	50.8	15.4	17.3	17.3
h-O-2	69 ± 5	83.8	82.5	41.6	55.9	54.2	22.3	20.4	20.4

(continued)

Table 4. (continued).

Composite Label	ν_{12}			ν_{23}			ν_{13}		
	Expt.	OA[a]	OAW[b]	Expt.	OA[a]	OAW[b]	Expt.	OA[a]	OAW[b]
l-L-1	0.024	0.023			0.216		0.22	0.607	
l-L-2	0.11	0.027	.037		0.310	.225	0.50	0.457	.436
l-T-1	0.048	0.020	.022		0.243	.200	0.375	0.541	.527
l-T-2	0.21	0.027	.031		0.325	.267	0.37	0.428	.406
l-O	0.053	0.034	.032		0.183	.180	0.49	0.184	.173
h-L-1	0.061	0.034	.041		0.266	.237		0.456	.450
h-L-2	0.13	0.035	.065		0.298	.221	0.45 ± .05	0.425	.411
h-T-1	0.054	0.033	.035		0.248	.240		0.486	.483
h-T-2	0.097	0.033	.036		0.280	.262		0.443	.437
h-O-1	0.055	0.051	.054		0.192	.184		0.190	.189
h-O-2	0.07	0.052	.052		0.158	.156		0.157	.155

(continued)

Table 4. (continued).

Composite Label	G_{12} (GPa)			G_{23} (GPa)			G_{31} (GPa)		
	Expt.	OA[a]	OAW[b]	Expt.	OA[a]	OAW[b]	Expt.	OA[a]	OAW[b]
l-L-1		2.3	—		2.1	—		6.0	—
l-L-2		2.4	2.4		2.2	2.2		3.2	3.2
l-T-1		3.0	3.0		2.7	2.7		5.6	5.6
l-T-2		2.6	2.6		2.4	2.4		3.1	3.1
l-O		3.1	3.1		2.8	2.8		2.7	2.7
h-L-1	6.2[c]	5.4	5.4		4.1	4.1		7.1	7.1
h-L-2	5.8[c]	4.6	4.6		3.6	3.6		5.3	5.3
h-T-1	5.6[c]	5.3	5.3		4.0	4.0		7.8	7.8
h-T-2	5.7[c]	5.0	5.0		3.9	3.9		6.2	6.2
h-O-1	5.0[c]	5.4	5.4		4.1	4.1		4.7	4.7
h-O-2		4.9	4.9		4.0	4.0		4.4	4.4

[a]Orientation Averaging Model of Section 3.2: straight fibers.
[b]Orientation Averaging Model amended for out-of-plane waviness of stuffers and fillers.
[c]Reference [27].

all fibers are aligned are treated as unidirectional composites. The whole composite becomes a 3D tessellation of transversely isotropic grains or domains whose orientations depend on the reinforcement architecture. Macroscopic properties are evaluated by averaging the response of the body to applied loads, usually under the assumption of either uniform stresses or, more often and more successfully, uniform strains. Such models are not particularly good for polycrystals containing highly anisotropic grains. It is likely that they owe their success for the continuous fiber composites studied so far to the high degree of long-range order that exists therein among the orientations of small volumes of fibers. Whether they will serve well in 3D composites containing short segments of multi-oriented tows remains to be assessed.

PROPERTY ESTIMATES FOR INDIVIDUAL TOWS

The properties of the individual domains, i.e., of a unidirectional composite, can be estimated from the local fiber volume fraction and the fiber and matrix properties. In this work, five different closed form approximations were assessed for estimating the properties of unidirectional composites, including rules of mixtures and four models from the literature which offer more realistic partitioning of stress between fibers and matrix [20,28–30]. Each method offers estimates in terms of the elastic constants of the fibers and resin of the five independent elastic constants available for the unidirectional composite when it is considered to be a transversely isotropic body. Of the five models, only Hashin's composite cylinder model [28] permits transverse isotropy in the fibers themselves; all the others treat the fibers as isotropic.

The resin and fiber properties used in this study are listed in Table 5. The prop-

Table 5. Fiber and resin elastic constants.

Fibers	Axial Young's Modulus E_f (GPa)	Axial Poisson's Ratio ν_f	Axial Shear Modulus G_f (GPa)	Transverse Young's Modulus E_{ft} (GPa)	Transverse Poisson's Ratio[a] ν_f
AS4 graphite fibers	235 (250)	0.25	55	17	0.27
S-2 glass fibers	85	0.22	—[b]	—[b]	—[b]

Resin	Young's Modulus E_r (GPa)	Poisson's Ratio ν_f
Tactix 138	3	0.3
Shell 1895	3.7	0.3

[a]Poisson's ratio in planes of isotropy.
[b]S2 glass assumed isotropic.

erties of the resins were measured in References [12] and [13]. The properties of S2 glass fibers, which are assumed isotropic, were taken from the literature [26] and manufacturer's data sheets.[8] The properties of AS4 carbon fibers, which are far from isotropic, were deduced by Naik [31] from the measured properties of a unidirectional AS4/3501-6 composite with $V = 0.6$ (Hercules[9] data sheet) using a finite element model of a composite of fibers in a square array. (Choosing a square array is hardly ideal, since it violates isotropy normal to the fibers. However, ensuing estimates of the properties of 3D composites will not be noticeably affected by such a minor consideration, as will become apparent below.) The value given in parentheses for the axial modulus of AS4 fibers is that given independently in the manufacturer's data sheets for bare AS4 fibers.[9]

Details of a comparison of the different models for the unidirectional composite are presented in Appendix B. Young's modulus and Poisson's ratio for loading in the fiber direction are essentially the same for all models and well approximated by the rule of mixtures. However, the transverse modulus, Poisson's ratio in the plane of isotropy, and the shear moduli all change significantly when the fiber anisotropy is taken into account. Therefore, Hashin's model with anisotropic fiber properties was used in further modeling.

ORIENTATION AVERAGING—IDEAL GEOMETRY

For orientation averaging, each 3D woven composite is divided into stuffer, filler, and two warp weaver domains occupying fractions A_α of the total composite volume ($\alpha = s, f, w_1$, or w_2 for stuffer, filler, or either weaver domain; $\Sigma_\alpha A_\alpha = 1$).

Each domain is characterized by an orientation along which the fibers within it are presumed to lie. Tow waviness does not enter into the definition of these orientations, but will be introduced separately. Thus all fibers within the stuffer or filler domains are assumed to be parallel to the x_1-axis or x_2-axis respectively. While warp weavers are always assumed to be piecewise straight and lie within x_1-x_3 planes, their orientations are defined differently for angle and orthogonal interlock weaves. For angle interlock weaves, the fibers occupying domain w_1 form an angle of 45° with the x_1-axis; while the fibers occupying domain w_2 form an angle of $-45°$ with the x_1-axis. In angle interlock weaves, domains w_1 and w_2 are occupied by equal numbers of fibers. For orthogonal interlock weaves, domains w_1 and w_2 are assumed to contain fiber segments parallel to the x_1 axis and parallel to the x_3 axis respectively in the proportions a_1:t in composite h-O-1 or $2a_1$:t in composites l-O or h-O-2, where a_1 is the center-to-center spacing of fillers ($a_1 \approx 1/p$). The assignment of orientations for the warp weavers is crude but adequate, because their contribution to overall properties is limited by their relatively low volume fraction.

Let $C^{(\alpha)}$ denote the stiffness matrix for domain α, i.e., the matrix of stiffness constants determined for the appropriate unidirectional composite by Hashin's

[8]Owens Corning Glass Co., Detroit, Michigan.
[9]Hercules Inc., Salt Lake City, Utah.

model in the local coordinate system (x,y,z) in which the x-axis lies along the fiber direction. The composite stiffness matrix C is approximated by

$$C_{ij} = \sum_{\alpha} A_\alpha \overline{C}_{ij}^{(\alpha)} \tag{9}$$

where $\overline{C}^{(\alpha)}$ denotes $C^{(\alpha)}$ transformed into the composite coordinate system (x_1,x_2,x_3) of Figure 1. This transformation is a well-known result of tensor algebra [32]. Equation (9) is an exact representation of the composite if all three domains $\alpha = s, f$, and $w = w_1 \cup w_2$ suffer equal strains under macroscopically uniform applied loads. Whether domain strains are in fact equal depends on the reinforcement architecture and the state of applied stress. An assessment of the effect of using other assumptions about the distribution of domain strains is deferred to the Discussion.

Equation (9) and Hashin's model for estimating $C^{(\alpha)}$ allow the composite elastic constants C to be estimated from the properties of the constituent fibers and resin. The solutions are closed by specifying the domain volume proportions A_α. In practice, it is difficult to specify A_α a priori, because of the complex geometry of resin pockets and voids between tows. In the following work, A_α was simply equated to the fiber fraction f_α of Table 2. To justify this assignment, the sensitivity of estimates of composite elastic constants to the choice of A_α was assessed by varying A_s with $A_w = f_w$, $\Sigma_\alpha A_\alpha = 1$, and total fiber fractions preserved by setting $V_\alpha = f_\alpha V/A_\alpha$ (with V the measured total fiber volume fraction). Within the bounds imposed on A_s by requiring $V_\alpha \leq 0.8$ for each domain, no composite elastic constant deviated by more than $\sim 2\%$.

Engineering elastic constants computed via Equation (9) and using Hashin's model for anisotropic fibers are compared with the experimental measurements in Table 4. Agreement is excellent for the shear modulus G_{12} and good for most other entries. However, the in-plane Young's moduli E_1 and E_2 are consistently overestimated by the orientation averaging model, while the in-plane Poisson's ratio ν_{12} is underestimated. The through-thickness modulus E_3 and Poisson's ratio ν_{13} are significantly high in some cases and significantly low in others. Nearly all of these variances can be attributed to geometrical irregularity.

THE INFLUENCE OF STUFFER AND FILLER WAVINESS

The most important effect of tow waviness on elastic properties is to reduce the axial stiffness of a tow. In the Orientation Averaging model, Young's modulus in the fiber direction in domain α is knocked down by a factor $\eta^{(\alpha)} \leq 1$, which can be estimated from the distribution of out-of-plane misalignment angles. Consider an axially loaded wavy tow as a sequence of misoriented unidirectional composite segments bearing equal stresses in the load direction.[10] The spatially averaged

[10]Detailed simulations of load distributions confirm the validity of assuming uniform stress along an individual wavy tow, rather than uniform strain [22]. However, the differences found in waviness effects when Equation (10) is based on isostrain conditions in a wavy tow are minor (zero to order ξ^2) [22]. Appendix A of Reference [21] also demonstrated that the highly anisotropic tows in typical polymer composites deflect laterally by shear rather than bending; and this is a much more important distinction. Thus the analysis preferred here differs from that appropriate to isotropic wavy layers in a soft matrix [33].

Young's modulus $\langle E_x^{(\alpha)} \rangle$ of such a tow is given by

$$\langle E_x^{(\alpha)} \rangle = \left\{ \int_{-\infty}^{\infty} \frac{f_\xi(\xi)\, d\xi}{\bar{E}_x^{(\alpha)}(\xi)} \right\}^{-1} \tag{10}$$

where $\bar{E}_x^{(\alpha)}(\xi)$ is Young's modulus for a unidirectional composite under a load oriented at angle ξ to the fiber direction x. A simple and adequate expression for $\bar{E}_x^{(\alpha)}(\xi)$ is [26].

$$1/\bar{E}_x^{(\alpha)}(\xi) = \frac{\cos^4 \xi}{E_x^{(\alpha)}} + \cos^2 \xi \sin^2 \xi \left(\frac{1}{G_{xy}^{(\alpha)}} - \frac{2\nu_{xy}^{(\alpha)}}{E_x^{(\alpha)}} \right) + \frac{\sin^4 \xi}{E_y^{(\alpha)}} \tag{11a}$$

$$\approx \frac{1}{E_x^{(\alpha)}} + \left(\frac{1}{G_{xy}^{(\alpha)}} - \frac{2(1 + \nu_{xy}^{(\alpha)})}{E_x^{\alpha}} \right) \xi^2 \quad \text{(small } \xi\text{)} \tag{11b}$$

where $E_x^{(\alpha)}$, $E_y^{(\alpha)}$, $G_{xy}^{(\alpha)}$, and $\nu_{xy}^{(\alpha)}$ are engineering elastic constants for a unidirectional composite when load and fibers are both aligned along the x-axis. With the integral in Equation (10) evaluated for f_ξ of Equation (5b), the knockdown factor $\eta^{(\alpha)}$ is just

$$\eta^{(\alpha)} = \langle E_x^{(\alpha)} \rangle / E_x^{(\alpha)} \tag{12a}$$

$$\approx \left\{ 1 + \sigma_\xi^2 \left[\frac{E_x^{(\alpha)}}{G_{xy}^{(\alpha)}} - 2(1 + \nu_{xy}^{(\alpha)}) \right] \right\}^{-1} \quad \text{(small } \sigma_\xi\text{)} \tag{12b}$$

The term multiplying σ_ξ^2 in Equation (12b) vanishes if the domain α is isotropic. It takes a value near 40 for the composites studied here. Equations (11b) and (12b) fall within 5% of Equations (5b), (10), and (11a) for $\sigma_\xi \leq 10°$. For smaller angles, Equation (12b) can be further simplified to

$$\eta^{(\alpha)} \approx 1 - \sigma_\xi^2 \left[\frac{E_x^{(\alpha)}}{G_{xy}^{(\alpha)}} - 2(1 + \nu_{xy}^{(\alpha)}) \right] \tag{12c}$$

Waviness knockdown factors computed for stuffers and fillers without the approximations of Equation (12b) or (12c) are listed in Table 3. The stiffness loss is 2–20% for stuffers and 5–50% for fillers.

Waviness knockdowns for stuffers and fillers are incorporated in the estimates for 3D woven composite properties by substituting $E_x^{(\alpha)} \to \eta^{(\alpha)} E_x^{(\alpha)}$ and $\nu_{xy}^{(\alpha)} \to \eta^{(\alpha)} \nu_{xy}^{(\alpha)}$ in the stuffer and filler domains in the Orientation Averaging Model. The latter substitution preserves the symmetry relations between Young's moduli and Poisson's ratios. The resulting composite predictions are listed in Table 4 under the heading "OAW." The agreement with experimental data is significantly improved. In many cases, the remanent discrepancy between prediction and experiment is less than the scatter in the experimental data and in data reported by

different laboratories for the same materials. Nevertheless, in many cases, the predicted in-plane Young's moduli remain higher than the experimental data.

THE INFLUENCE OF WARP WEAVER CRIMP

Since warp weaver crimp is so severe, a meaningful lower bound to its effect can be found by the extreme assumption that the axial modulus $E_x^{(w)}$ of the warp weavers is reduced to the value $E_z^{(w)}$ of their transverse modulus. Symmetry relations are preserved by the substitution $\nu_{xy}^{(w)} \rightarrow \nu_{yz}^{(w)}$. Some composite elastic constants predicted with these conditions are compared in Table 6 with predictions for warp weavers of ideal geometry. Young's modulus E_1 is only weakly affected by weaver crimp, as is E_2 (not shown in Table 6). The through-thickness modulus E_3, Poisson's ratio ν_{13}, and the shear modulus G_{31} are more substantially affected,

Table 6. Effects of warp weaver crimp.

Composite Label	E_1 (GPa)		E_3 (GPa)	
	OAW[a]	OAWW[b]	OAW[a]	OAWW[b]
l-L-1	36.8	35.7	9.0	5.6
l-L-2	29.4	28.9	6.9	5.9
l-T-1	41.3	40.2	9.4	6.7
l-T-2	37.1	36.8	7.0	6.2
l-O	45.5	42.1	13.7	6.9
h-L-1	88.6	87.6	12.1	9.7
h-L-2	77.6	77.0	10.2	8.8
h-T-1	87.0	85.7	12.8	9.6
h-T-2	82.4	81.6	11.2	9.3
h-T-1	93.0	90.0	17.3	9.6
h-O-2	82.5	80.0	20.4	9.2

Composite Label	ν_{13}		G_{31} (GPa)	
	OAW[a]	OAWW[b]	OAW[a]	OAWW[b]
l-L-1	0.607	0.323	6.0	2.2
l-L-2	0.436	0.320	3.2	2.3
l-T-1	0.527	0.306	5.6	2.6
l-T-2	0.406	0.325	3.1	2.4
l-O	0.173	0.310	2.7	2.7
h-L-1	0.450	0.299	7.1	4.7
h-L-2	0.411	0.313	5.3	4.0
h-T-1	0.483	0.294	7.8	4.6
h-T-2	0.437	0.311	6.2	4.3
h-O-1	0.189	0.317	4.7	4.7
h-O-2	0.155	0.308	4.4	4.4

[a]Orientation Averaging Model amended for out-of-plane waviness of stuffers and fillers.
[b]As for OAW but with extreme softening of warp weavers.

falling to values near those expected for a 2D laminate. Other Poisson's ratios and shear moduli are insignificantly affected.

BENDING

For many purposes, it will be accurate enough to represent any of the 3D woven composites studied here as orthotropic and homogeneous. However, in bending applications, the coarseness of typical tows suggests that account must be taken of the sequence in which stuffers and fillers appear through the thickness (Figure 2). This effect can be measured as the ratio χ_j ($j = 1,2$) of the flexural rigidity estimated for the actual layer sequence to that estimated under the assumption of through-thickness homogeneity. The required ratio follows easily from the distribution of layer stiffnesses and stresses in pure bending.[11] For a symmetric through-thickness sequence and bending about the x_j-axis ($j = 1,2$), the bending moment M_j is given by

$$M_j = \int_{-t/2}^{t/2} \sigma_j(x_3) x_3 dx_3 \tag{13}$$

Ignoring the modest effect of transverse stresses, the ratio χ_j is well approximated by

$$\chi_j = \frac{4}{3t} \sum_{i=1}^{n_s+1} (u_i^3 - u_{i-1}^3) E_j^{(\alpha_i)} \Big/ \frac{t^2}{6} E_j \tag{14a}$$

$$= \sum_{i=1}^{n_s+1} \left[\left(\frac{u_i}{t/2} \right)^3 - \left(\frac{u_{i-1}}{t/2} \right)^3 \right] E_j^{(\alpha_i)} / E_j \quad (j = 1,2) \tag{14b}$$

where E_j is Young's modulus in direction x_j for the composite; and $E_j^{(\alpha_i)}$ is Young's modulus in direction x_j for the individual layer (or tow domain) α_i. The moduli $E_j^{(\alpha_i)}$ are either the axial or transverse Young's modulus predicted for a unidirectional composite; the former knocked down by the factor $\eta^{(\alpha_i)}$ to allow for tow waviness.

Values computed for χ_j by Equation (14) are summarized for all the composites in Table 7. Since fillers are always the outermost plies, χ_2 exceeds unity (bending about the x_1-axis) while χ_1 is less than unity (bending about the x_2-axis).

Given χ_1 and χ_2, the flexural rigidities E_{f1} and E_{f2} that should be used to predict the response to pure bending under the assumption that the composite is homogeneous can be estimated from the in-plane moduli E_1 and E_2. Results for E_{f1} are compared in Table 7 to values deduced from the linear portions of bending

[11]The ratio χ_j is to be applied as a correction factor to the OAM, which already contains estimates of the effects of warp weavers. The influence of warp weavers on the correction factor itself must be negligible.

Table 7. Flexural rigidity.

Composite Label	Factor for Inhomogeneity		Flexural Rigidity E_{fl}[a] (MPa)	
	χ_1[a]	χ_2[b]	Expt.	Prediction[c]
l-L-1	0.79	1.19	20	29
l-L-2	0.78	1.15	—	23
l-T-1	0.78	1.17	—	32
l-T-2	0.79	1.18	—	29
l-O	0.78	1.17	—	35
h-L-1	0.85	1.24	72	75
h-L-2	0.89	1.14	—	69
h-T-1	0.85	1.25	63	74
h-T-2	0.89	1.16	63	73
h-O-1	0.84	1.25	60	78
h-O-2	0.89	1.16	—	73

[a]Bending about the x_2-axis.
[b]Bending about the x_1-axis.
[c]Equation (14).

experiments. The predictions (which contain no knockdown for tow waviness) are consistently higher than the available data. The discrepancy can be attributed to overestimates in E_1, since the proportional discrepancies in E_1 (Table 4) and E_{f1} (Table 7) are nearly the same. Thus, the effects of inhomogeneity are well estimated by Equation (14).

4. DISCUSSION

4.1 In-Plane Properties

The in-plane elastic properties are essentially those of a 0°/90° laminate, with relatively minor modifications due to the through-thickness reinforcement and tow irregularity. Thus Poisson's ratio ν_{12} is very small, because the fillers resist transverse contraction when loading is parallel to the stuffers; and ν_{12} and the in-plane Young's moduli E_1 and E_2 are dominated by the axial stiffness of the stuffers and fillers. Consequently, using rules of mixtures rather than Hashin's model for tow domain properties leads to very similar predictions of the composite elastic constants E_1, E_2, and ν_{12} (Appendix B). On the other hand, the in-plane shear modulus G_{12} is matrix dominated: it is very nearly equal to the axial shear modulus predicted for the stuffers and fillers. The rule of mixtures leads to an underestimate for G_{12} (Appendix B).

The in-plane elastic constants E_1, E_2, and ν_{12} are influenced significantly by waviness in stuffers and fillers, but negligibly by waviness in the warp weavers.

4.2 Other Elastic Constants

The orientation of the warp weavers and any crimp in them is much more significant for the through-thickness composite modulus E_3, Poisson's ratios ν_{13} and ν_{23}, and the shear modulus G_{31}. As tow orientations would suggest, the highest values of E_3 are found for orthogonal interlock weaves. Similarly, ν_{13} and ν_{23} are less than Poisson's ratio for the matrix for orthogonal interlock weaves, but are quite high in angle interlock weaves. The warp weavers resist through-thickness contraction in the former architecture, but abet it in the latter. Of the shear moduli, only G_{31} depends on the warp weavers: no axial strains arise in any segments of warp weavers under shear strains γ_{12} or γ_{23}.

4.3 Unresolved Discrepancies between Theory and Experiment

When out-of-plane stuffer and filler waviness and warp weaver crimp are accounted for, predicted and measured composite elastic constants agree in most cases to within experimental error. However, the tendency is still for predicted in-plane Young's moduli to be too high, especially for composites *l*-T-1, *l*-0, and *h*-O-2; while experiment and theory occasionally disagree significantly in either direction for the through thickness modulus E_3 and Poisson's ratio ν_{13}.

The remaining overestimate of in-plane moduli is very likely to arise from unaccounted irregularity in stuffers and fillers. Only out-of-plane waviness was measured and modeled, yet other forms of distortions can also be found. Many consist of inconstancy in the aspect ratios of tow cross sections. In some composites, especially layer-to-layer angle interlocks, this was manifested as tapering, oscillating skirts along the sides of stuffers or fillers, giving them a shape reminiscent of long flatworms. In all composites, aspect ratios are also disrupted by "pinching," i.e., locations where a tow is flattened by lateral loads during processing. Other possible irregularities include yarn twist, which is assumed zero in accord with the weaver's specifications; and in-plane waviness. Unfortunately, it is *virtually impossible* to measure all such irregularities, or even to identify them clearly in specimens. Indeed there will very likely always be some uncertainty in the degree of irregularity existing in textile composites. It is consequently unrealistic to expect to predict even in-plane elastic constants to within better than $\sim 10\%$.

While a 10% uncertainty will usually be deemed quite acceptable in a prediction based on constituent properties, the situation for out-of-plane properties is more challenging. Three distinct problems exist. (1) The isostrain assumption is wrong in the through-thickness direction, as clearly borne out by moiré data such as Figure 8(b). Model calculations that allow a natural partitioning of loads between warp weavers and the rest of the composite appear in Reference [22]. They demonstrate that the isostrain assumption exaggerates the influence of warp weavers, by not allowing the rest of the composite to relax around them. (2) The crimp factor c_w for warp weavers is difficult to measure and subject to considerable variance. Errors in specifying the spatial density of warp weaver fibers are the most plausible cause of predicted values of E_3 falling short of measured values (3) Waviness and other distortions are relatively severe for warp weavers.

Rough estimates show that the effects of warp weaver irregularity on E_3, ν_{13}, and G_{31} are of similar magnitude to the effects of relaxing the isostrain condition. Thus, when through-thickness property estimates are required in composite design, the simple Orientation Averaging Model with isostrain conditions might just as well be used, with suitably stated levels of uncertainty. Table 4 suggests that an uncertainty of $\sim 20\%$ is typical for current 3D woven composites.

5. CONCLUSIONS

Tow waviness has been analyzed experimentally in 3D woven composites. (1) The waviness found in nominally straight yarns varies considerably from stuffers to fillers and from specimen to specimen. It is generally much higher for fillers, which are not tensioned during weaving, than for stuffers, which are. It tends to be relatively high in the layer-to-layer architecture, intermediate in the through-thickness architecture, and least in the orthogonal interlock architecture. (2) Very large variation is found in the waviness of through-thickness interlock yarns (warp weavers). The most severely deformed warp weavers are found in composites subjected to large through-thickness compaction during consolidation.

Tow waviness has its most powerful effects on strength, ductility, and fatigue life [12–15]. Nevertheless, it can also have a significant effect on macroscopic elastic properties. Even for the heavily compacted composites studied here, which represent the state of the art, the knockdown in Young's modulus due to tow waviness can be 5% in the stuffer direction and 30–50% in the filler direction. These materials are far from optimal and will remain so until weavers and composite processors learn to control tow regularity. Control could be achieved by tow tensioning both in the loom and during resin infiltration and cure.

In analyzing macroscopic response to loads, it is a good approximation to regard the composites studied here as homogeneous over lengths exceeding 10 mm and orthotropic. The Orientation Averaging Model with simple corrections for tow waviness is an excellent method of predicting in-plane macroscopic elastic constants; and a fair method of estimating elastic constants related to through-thickness strains. For in-plane properties, the composites studied here behave macroscopically very nearly as 0°/90° laminates.

ACKNOWLEDGEMENTS

The authors gratefully acknowledge funding by NASA Langley Research Center under Contract No. NAS1-19243; the assistance of Mr. Scott Schroeder and Dr. Mike Shaw with some measurements; and useful discussions with Drs. Chris Pastore and James Singletary.

APPENDIX A. WEAVE PATTERNS

This index provides a few notes on the patterns of yarns found in the composites of Table 1, sufficient for evaluating macroscopic elastic properties. Complete statements of the quite complex sequencing of through-thickness yarns is deferred to Reference [22], which analyzes local fluctuations in load distribution. There knowledge of the detailed arrangement of yarns is essential.

In every composite, the stuffers and fillers form a coarse 0°/90° array. Stuffers and fillers alternate in layers through the thickness, with fillers always occupying the outermost layers. The through-thickness reinforcement, or warp weavers, traverse the thickness of the specimen in planes normal to the fillers. They bind together fillers in different layers as they turn around them (Figure A.1). The warp weavers also serve to hold the stuffers roughly in columns standing normal to the filler direction. The number of warp weavers between columns of stuffers, n_w, is usually one or two (see Reference [22] for details).

In angle interlock weaves, the warp weavers follow approximately sawtooth paths. Successive segments make angles of approximately 45° to the stuffer direction. In through-the-thickness angle interlock weaves, warp weavers turn around fillers in the outermost layers only [Figure A.1(b)]. In layer-to-layer angle interlock weaves, most warp weavers couple fillers in successive fillers; a few, lighter warp weavers oscillate entirely within either of the outermost layers of fillers [Figure A.1(a)].

In orthogonal interlock weaves, the warp weavers pass right through the specimen approximately at right angles to the stuffer direction [Figure A.1(c)]. In composite *h*-O-1, they pass around a single filler in the outer layer of fillers before reversing back through the thickness. In composites *l*-O and *h*-O-2, they pass around two fillers before reversing. Thus the warp-weavers in orthogonal interlock weaves follow approximately rectangular wave paths of height t, the specimen thickness, and half wavelength either a_1 (*h*-O-1 and *h*-O-2) or $2a_1$ (*l*-O), where a_1 is the center-to-center separation of fillers.

APPENDIX B. THE ELASTIC PROPERTIES OF UNIDIRECTIONAL FIBER COMPOSITES

This appendix provides further details of the use of existing models in the literature for estimating the elastic properties of unidirectional fibrous composites. In the following, V is the fiber volume fraction; E_r and ν_r are Young's modulus and Poisson's ratio for the resin; E_f and ν_f are Young's modulus and Poisson's ratio for the fibers under axial load; μ_f is the axial shear modulus of the fibers: E_{ft} is the transverse Young's modulus for the fibers; and ν_{ft} is Poisson's ratio for the fibers in their plane of isotropy.

The following five models of unidirectional composites were compared.

1. Rules of Mixtures [26]
2. Hill's Self-Consistent Method [29]
3. Christensen's Modified Self-Consistent Model [30]
4. Van Fo Fy's infinite series results for an hexagonal array [34], as simplified in Reference [20]
5. The average of Hashin's bounds for anisotropic fibers in an isotropic matrix [28]

Each model provides explicit expressions for the unidirectional composite elastic constants. In rules of mixtures, any composite property q_c is related to the corresponding constituent properties q_f and q_r by either

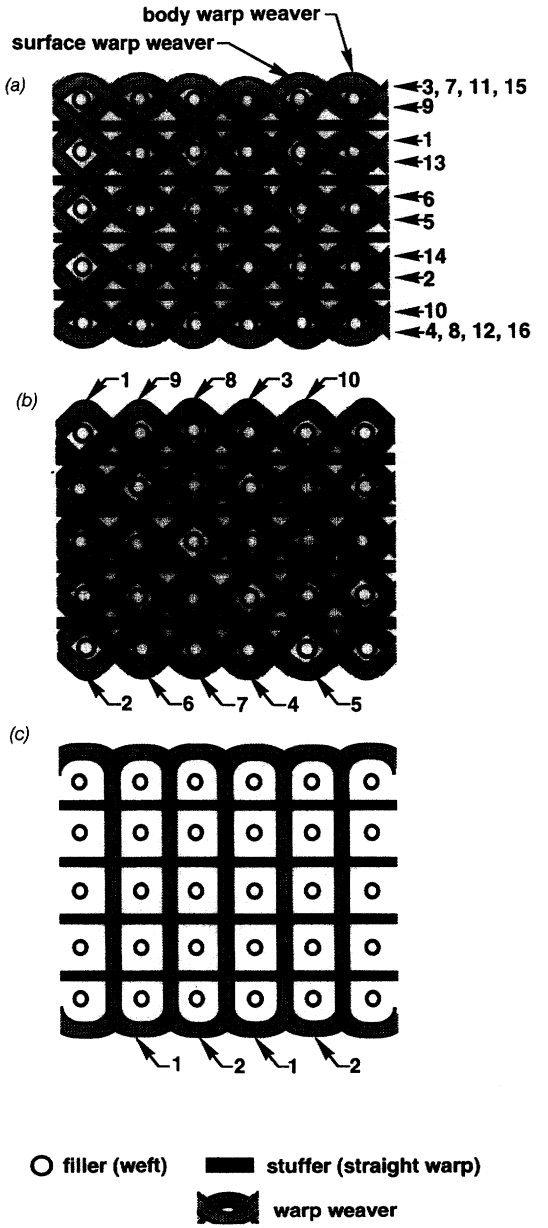

Figure A.1. *Schematics of the three 3D weave architectures studied in this work. (a) Layer-to-layer angle interlock. (b) Through-the-thickness angle interlock. (c) Orthogonal interlock. The numbers indicate the order in which warp weavers are encountered in progressing down the filler direction.*

$$q_c = Vq_f + (1 - V)q_r \tag{B.1a}$$

or

$$q_c = [V/q_f + (1 - V)/q_r]^{-1} \tag{B.1b}$$

with Equation (B.1a) used for the axial Young's modulus and Poisson's ratios and Equation (B.1b) for the transverse Young's modulus and shear moduli. For models 2–5, the reader is referred to the cited references for the relevant formulae, which are straightforward but lengthy to write out. A computer program for their evaluation can be obtained from the authors.

Properties estimated using the constituent properties of Table 5 for a unidirectional composite of AS4 fibers in Shell 1895 resin are compared as functions of fiber volume fraction for each of the approximations 1–3 and 5 in Figure B.1. For models 1–3, where the fibers are assumed isotropic, only the axial modulus E_f

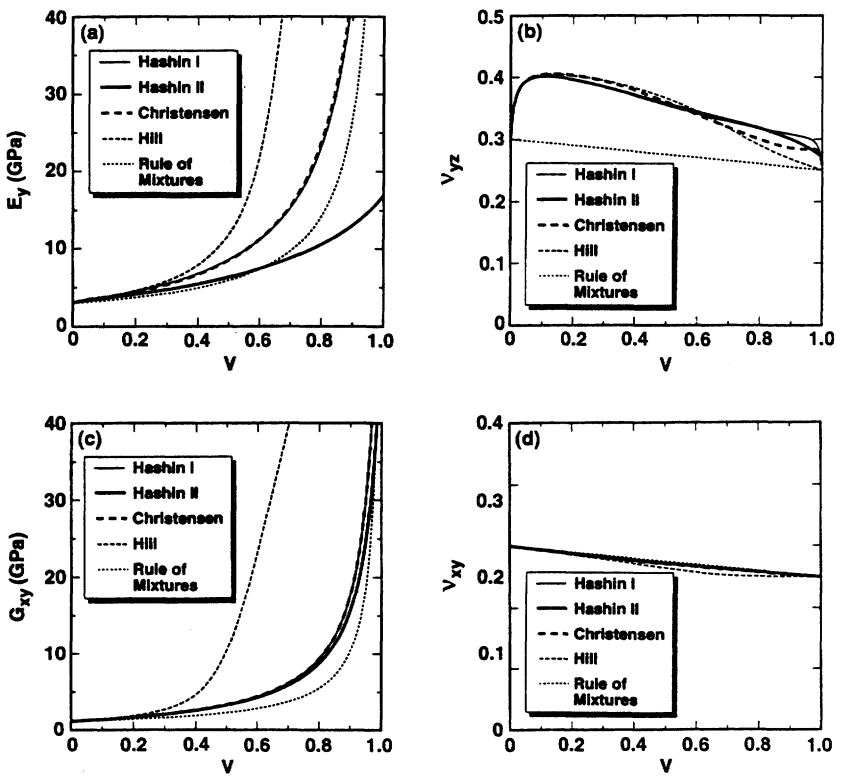

Figure B.1. *Comparison of the elastic constants predicted for a unidirectional AS4/1895 composite using various models from the literature.*

Table B.1. Comparison of estimates of 3D composite elastic constants for composite h-L-1 using different models for domain properties.

Model for Domain Properties	E_1 (GPa)	E_2 (GPa)	G_{12} (GPa)	ν_{12}	E_3 (GPa)
Rule of Mixtures[a]	91.6	56.7	3.7	0.037	12.4
Hill [29][a]	102.1	70.3	26.6	0.11	34.5
Christensen [30][a]	93.8	60.2	5.7	0.056	17.9
Van Fo Fy [34][c]	93.3	59.5	5.7	0.053	17.3
Hashin [28] I[a]	93.7	60.1	5.7	0.056	17.9
Hashin [28] II[b]	91.5	56.2	5.4	0.034	12.1

[a]For isotropic fibers with E_f and ν_f as in Table 4.
[b]For anisotropic fibers.
[c]With simplifications of Gowayed and Pastore [20].

and axial Poisson's ratio ν_f were used in producing this figure. For Hashin's model, estimates were made for both isotropic and anisotropic fibers. Results for model 4 are not plotted because they are very close to those from Christensen's method, except near $V = 0$ and $V = 1$, where some accuracy was lost in the simplified expressions given in Reference [20].

Among all the cases, no discrepancy is found in the axial modulus, E_x, which was therefore not plotted. It is given very accurately by the rule of mixtures. In contrast, some significant discrepancies are found in transverse and shear moduli and Poisson's ratio in the plane of isotropy. In rules of mixtures, transverse properties and Poisson's ratios are estimated by partitioning stresses between the fibers and resin as though they were arranged in layers [26]. The estimates given by rules of mixtures for transverse modulus and shear moduli are consequently less than those in the other models, in which the fiber geometry is treated more accurately. All of the approximations give very similar results for composites of isotropic fibers at low volume fraction, V. Hill's method gives answers for transverse and shear properties that are much too high when $V \gtrsim 0.3$ and the fibers are much stiffer than the matrix, which is almost universally the case for polymer composites. Christensen's self-consistent model and Hashin's composite cylinder model give similar results for composites with isotropic fibers. However, as the data of Table 5 show, graphite fibers are highly anisotropic. Thus, the shear and transverse moduli shown in Figure B.1 for Hashin's model for anisotropic fibers are much lower than those for models 2 and 3. Indeed, for $0.4 \leq V \leq 0.6$ all constants except the axial shear modulus are fortuitously rather close to the rule of mixtures predictions.

Engineering elastic constants were then estimated for each 3D woven composite using the constituent properties of Table 5 and all five methods of estimating domain properties. Some representative constants computed for composite *h*-L-1 are compared in Table B.1. Barring the results from Hill's model, which is clearly wrong for such high volume fractions, there are only quite small variations among the different entries for any property. The estimates following from rules

Table B.2. Computed tow domain properties.

Composite Label	Stuffers/Fillers					Warp Weavers				
	E_x (GPa)	E_y (GPa)	ν_{xy}	G_{xz} (GPa)	ν_{yz}	E_x (GPa)	E_y (GPa)	ν_{xy}	G_{xz} (GPa)	ν_{yz}
(a) Lightly Compacted										
l-L-1	84.2	5.11	0.280	2.32	0.378	5.11	5.11	0.280	2.32	0.378
l-L-2	88.8	5.25	0.279	2.42	0.375	6.13	6.13	0.264	2.37	0.365
l-T-1	111.1	6.04	0.274	3.02	0.362	6.04	6.04	0.274	3.02	0.362
l-T-2	97.6	5.54	0.277	2.64	0.370	6.62	6.62	0.261	2.57	0.360
l-0	115.1	6.19	0.273	3.14	0.360	6.19	6.19	0.273	3.14	0.360
(b) Heavily Compacted										
h-L-1	147.1	8.72	0.267	5.50	0.340	8.72	8.72	0.267	5.50	0.340
h-L-2	132.5	7.98	0.270	4.62	0.349	7.98	7.98	0.270	4.62	0.349
h-T-1	145.5	8.63	0.267	5.39	0.341	8.63	8.63	0.267	5.39	0.341
h-T-2	140.6	8.38	0.268	5.08	0.344	8.38	8.38	0.268	5.08	0.344
h-O-1	146.9	8.71	0.267	5.48	0.340	8.71	8.71	0.267	5.48	0.340
h-O-2	140.9	8.39	0.268	5.09	0.344	8.39	8.39	0.268	5.09	0.344

Note: the x axis lies in fiber direction, with the y and z axes forming planes of isotropy.

of mixtures and Hashin's model with anisotropic fiber properties are especially close for every engineering constant, including those not shown in Table B.1, with the single exception of the in-plane shear modulus G_{12}, where a 30% difference is found.

In the process of computing elastic constants for the composite, fiber volume fractions and elastic properties are also found for individual tow domains. These are given in Table B.2 for Hashin's model and the composite volume fractions, etc., of Tables 1, 2, and 5. Table B.2 does not include the effects of tow waviness.

REFERENCES

1. Bradshaw, F. J., G. Dorey and G. R. Sidey. 1973. "Impact Resistance of Carbon Fiber Reinforced Plastics," Tech. Rep. 72240, Royal Aircraft Establishment, England.
2. Novak, R. C. 1975. "Materials Variables Affecting the Impact Resistance of Graphite and Boron Composites–II," Rep. TR-74-196, Part II, U.S. Air Force Materials Laboratory, Dayton, OH.
3. McAllister, L. E. and W. L. Lachman. 1983. In *Fabrication of Composites, Handbook of Composites, Vol. 4.* New York: Elsevier, p. 109.
4. Guess, T. R. and E. D. Reedy, Jr. 1985. *J. Comp. Tech. Res.*, 7:136.
5. Reedy, E. D., Jr. and T. R. Guess. 1986. *J. Comp. Tech. Res.*, 8:163.
6. Mignery, L. A., T. M. Tan and C. T. Sun. 1985. In *Delamination and Debonding, ASTM Spec. Tech. Publ. 876,* W. S. Johnson, ed., Philadelphia, PA: ASTM, pp. 371–385.
7. Smith, P. J. and R. D. Wilson. 1985. "Damage Tolerant Composite Wing Panels for Transport Aircraft," NASA Contractor Report 3951, Boeing Commercial Airplane Company.
8. Chou, T.-W., R. L. McCullough and R. B. Pipes. 1986. "Composites," *Scientific American,* 254(10):193–203.
9. Ko, F. 1989. In *Textile Structural Composites; Composite Materials, 3,* T.-W. Chou and F. Ko, eds., New York: Elsevier, Chapter 5.
10. Horton, R. E. and J. E. McCarty. 1987. In *Engineered Materials Handbook, Vol. 1, Composites,* C. A. Dostal, ed., Metals Park, OH: Am. Soc. Metals.
11. Brandt, J., K. Dreschler and R. Meistring. 1990. "The Application of Three-Dimensional Fiber Preforms for Aerospace Composites," *Proc. ESA Symp. on Space Applications of Advanced Structural Materials,* ESTEC, Noordwijk, Netherlands, March (ESA SP-303, June, 1990), pp. 71–77.
12. Cox, B. N., M. S. Dadkhah, R. V. Inman, W. L. Morris and J. Zupon. 1992. "Mechanisms of Compressive Failure in 3D Composites," *Acta Metall. Mater.*, 40:3285–3298.
13. Cox, B. N., M. S. Dadkhah, W. L. Morris and J. G. Flintoff. 1994. "Failure Mechanisms of 3D Woven Composites in Tension, Compression, and Bending," *Acta Metall. Mater.*, 42:3967–3984.
14. Cox, B. N., M. S. Dadkhah and W. L. Morris. "On the Tensile Failure of 3D Woven Composites," submitted to *Composites*.
15. Dadkhah, M. S., B. N. Cox and W. L. Morris. "Compression-Compression Fatigue of 3D Woven Composites," *Acta Metall. Mater*, in press.
16. Tarnopol'skii, Y. M., V. A. Polyakor and I. G. Zhigun. 1973. "Composite Materials Reinforced with a System of Three Straight, Mutually Orthogonal Fibers, I: Calculation of Elastic Characteristics," *Polymer Mechanics,* 5:853–860.
17. Kregers, A. F. and Y. G. Melbardis. 1978. "Determination of the Deformability of Three-Dimensional Reinforced Composites by the Stiffness Averaging Method," *Polymer Mechanics,* 1:3–8.
18. Kregers, A. F. and G. A. Teters. 1981. "Determination of the Elasto-Plastic Properties of Spatially Reinforced Composites by the Averaging Method," *Mech. Comp. Mater.*, 17:25–31.

19. Yang, J.-M., C.-L. Ma and T.-W. Chou. 1986. "Fiber Inclination Model of Three-Dimensional Textile Structural Composites," *J. Composite Materials,* 20:472–484.
20. Gowayed, Y. A. and C. M. Pastore. 1991. "Analytical Techniques for Textile Structural Composites: A Comparative Study of US-USSR Research," *Fiber-Tex 90,* Clemson, SC, August 1990, *NASA Conf. Publ. 3128,* J. D. Buckley, ed., NASA.
21. Cox, B. N., W. C. Carter and N. A. Fleck. 1994. "A Binary Model of Textile Composites. I Formulation," *Acta Metall. Mater.*, 42:3463–3479.
22. Xu, J., B. N. Cox, M. A. McGlockton and W. C. Carter. "A Binary Model of Textile Composites: II The Elastic Regime," to *Acta Metall. Mater*, in press.
23. Cox, B. N., M. S. Dadkhah, R. V. Inman, J. Flintoff, M. R. Mitchell and W. L. Morris. 1993. "Design and Reliability Guide for Triaxially Braided Composites," Rockwell International Science Center, Report to Rockwell Plastic Products Division, November.
24. Cox, B. N., M. S. Dadkhah, M. R. Mitchell and T. W. Kniveton. "The Effects of Tow Waviness on the Stiffness, Strength, and Fatigue Life of Triaxially Braided Composites," to be submitted to *J. Comp. Mater.*
25. Wilks, S. S. 1962. *Mathematical Statistics.* New York: John Wiley and Sons.
26. Piggott, M. R. 1990. *Load-Bearing Fiber Composites.* Oxford: Pergamon, Chap. 1.
27. Ifju, P. G. Univ. Florida, private communication.
28. Hashin, Z. 1979. "Analysis of Properties of Fiber Composites with Anisotropic Constituents," *J. Appl. Mech.*, 46:543–550.
29. Hill, R. 1965. "Theory of Mechanical Properties of Fiber-Strengthened Materials—III. Self-Consistent Model," *J. Mech. Phys. Solids,* 13:189–198.
30. Christensen, R. M. 1990. "A Critical Evaluation for a Class of Micromechanics Models," *J. Mech. Phys. Solids,* 38:379–404.
31. Naik, R. 1992. NASA Technical Memorandum.
32. Love, A. E. H. 1944. *A Treatise on the Mathematical Theory of Elasticity.* New York: Dover, Articles 12 and 49.
33. Lee, J.-W. and C. E. Harris. 1990. "A Deformation-Formulated Micromechanics Model of the Effective Young's Modulus and Strength of Laminated Composites Containing Local Ply Curvature," *ASTM STP 1059,* S. P. Garbo, ed., Philadelphia: ASTM, pp. 521–563.
34. Van Fo Fy, G. A. 1966. *Polymer Mechanics,* 2:593–602.